Progress In Electromagnetics Research C, Vol. 118, 1–10, 2022

A Novel Surface Wave Diplexer Based on Tensor Impedance Surfaces

Mojtaba Mighani*

Abstract—In this paper, a new Surface Wave (SW) diplexer in frequency bands of 11.6 GHz and 19.3 GHz is presented based on the frequency variations of the refractive angle when an SW enters from a Scalar Impedance Sheet (SIS) to a Tensor Impedance Sheet (TIS). In this structure, a SIS has been placed alongside a TIS, and using three launchers, SW is excited and received on them. To achieve an SW diplexer, the structure is designed in a way that the refractive angle changes in the expected range when SW enters from SIS to TIS. Finally, the proposed structure is fabricated and measured by printed circuit technology. The measurement results at 11.6 GHz and 19.3 GHz show that this structure has 3.6 dB and 4.1 dB insertion losses and 33.5 dB and 37 dB isolations in the two bands, respectively. These measurements are in good agreement with mathematical modelling and simulations.

1. INTRODUCTION

Diplexers are one of the most compelling three-port elements in microwave systems. One application of these devices is the simultaneous connection of a transmitter and a receiver with two different frequencies to an antenna [1]. Therefore, a diplexer can be used when we need to combine or separate two frequency channels, and a multiplexer is utilized for more than two channels. In other words, multiplexers and diplexers have a function similar to power combiners and splitters with the difference that unlike them, combiners and splitters can only be used in one frequency [2, 3]. Moreover, multiplexers have two major advantages compared to power splitters and combiners. First, they do not have the intrinsic attenuation of power combiners and splitters, and second, they can create isolation between their ports [4]. This behaviour makes multiplexers and diplexers highly efficient in multi-channel receivers. A diplexer can also be compared to a circulator. A diplexer can simultaneously operate in two separate channels. Therefore, it is more suitable than a circulator in many applications.

The design method of diplexers is usually based on connecting two filters with two different passbands via a T-junction. In this method, the most important problem is that each filter in the other filter passband must be an open connection. There are two methods for the diplexer design. One is usually based on optimizing an error function, which is a time-consuming process [5, 6], and the other is analytical methods based on the design of two separate filters and a coupling matrix [7, 8]. The fabrication methods of diplexers are based on printed circuit technology [7–11] and waveguides [12, 13]. In [10], an input reflectionless low-pass filter was presented, which consists of a reflective network implemented with a microstrip resonator and a resistive termination, and in [8], a switchable diplexer was presented by using pin diodes. The main advantages of printed circuit-based diplexers are the simplicity of construction and the possibility of combining with the lumped elements. On the other hand, the fabrication of diplexers with waveguides allows achieving low insertion losses and high-quality factors. For example, in [13], a waveguide-based diplexer with a 0.39 dB insertion loss and very high rejection was presented. Moreover, due to the high power handling, waveguide-based diplexers are more commonly used in transmitters.

Received 2 December 2021, Accepted 17 January 2022, Scheduled 18 January 2022
* Corresponding author: Mojtaba Mighani (microwave@ssau.ac.ir).
The author is with the Shahid Sattari Aeronautical University of Science and Technology, Iran.

In surface impedance structure, periodic unit cells are used to achieve the desired surface impedance properties. In SIS the cells are symmetric, and these cells will become asymmetric in one or both axes of the cells. Ideally, the number of these cells should be infinite, but usually when the number of repetitions is more than 10, the structure can be assumed to be almost periodic, and the boundary conditions can be approximated. The size and thickness of the cell must be small as compared to the wavelength. It is usually around $\lambda/10$ [14]. Unlike constitutive properties such as permittivity and permeability which are effects of the atomic structure of a material, impedance surfaces derive effective material properties from macroscopic periodic inclusions that are artificially added to a material.

Recently, using tensor impedance surfaces, a structure has been proposed that can be employed to design an SW diplexer [14–16]. The proposed structure is obtained by a TIS alongside a SIS and is designed using metallic arrays of cells over a grounded substrate. In this structure, an SW is excited on the SIS and orthogonally propagates onto the TIS due to the refraction phenomenon. The direction of propagation on the TIS will change due to SW frequency. In [14], the refraction angle changes were modelled according to the frequency and were validated on a sample structure with a range between 0 and 9 degrees at the 15.1–15.75 GHz frequency band. Moreover, in [15], the SW losses were modelled in this type of structure and included ohmic, dielectric, mismatch, and modes transform losses. With this method, the insertion losses between the input and the two output ports of the proposed diplexer can be calculated.

In this paper, the frequency variations of the refraction angle are used to present a new SW diplexer based on the TISs. Therefore, the SW is excited on the SIS by a launcher, which can include two frequency channels, and orthogonally propagates toward the boundary of the TIS as the incident wave. Now, according to the frequency of each channel, the SWs enter the TIS with different refractive angles, and the two bands will be separated from each other. Finally, these two SWs are received by using two launchers. The main advantage of this structure is the continuous change of the refraction angle in terms of SW frequency. This behaviour can enable the mechanical channel tuning in the structure by moving the SW launchers.

One of the most important challenges of using impedance sheets is the excitation and measurement of the SW on these surfaces. The simplest laboratory method is to use coaxial probes along the surface vertically and horizontally to excite transverse magnetic (TM) and transverse electric (TE) modes, respectively [17]. This method of testing, due to the low coupling efficiency, increases the insertion loss for a microwave device and is practically not usable. This approach is only applied when the goal is to validate the performance of a structure and the absolute value of the coupled power on the surface does not matter. For example, in [14] to validate the frequency changes of the refractive angle which were modelled by a new analytic method, coaxial probes were used.

The only practical way to overcome this limitation is to use SW launchers [18–24]. The launchers can couple the SW on the impedance surfaces with high efficiency. The design flaw of an SW launcher is that it needs a substrate with high relative permittivity, which limits the substrates that can be used for the launcher. For example, in theory, to achieve a coupling efficiency above 90%, a relative permittivity of higher than 10 is required [23, 24]. In [18, 19], an SW launcher was presented using a coplanar waveguide structure in such a way that it had an appropriate efficiency and frequency band. The size of the launchers varies depending on the defined parameters, for example in [18–19, 21], is $15 \times 15\,\mathrm{cm}^2$ at K-band frequency and in [22] is $7.5 \times 7.5\,\mathrm{cm}^2$ in X-band frequency. In our work, the structure proposed in [19] is used as a basis for designing the required launchers.

This paper consists of four sections. After the introduction, the design process of isotropic and anisotropic cells is described. This process is very important for the implementation of the required boundary conditions of SIS and TIS using printed circuit board (PCB) technology. In the third section, the losses on the presented structure are investigated. The structure is presented as a microwave diplexer; therefore, the loss calculation is essential. Finally, in the fourth section, the findings of the design and simulation are tested and measured.

2. SIS AND TIS DESIGN

Figure 1 shows how the proposed structure works. In this structure, three launchers are used as input and output ports in two frequency bands. For the proposed structure, appropriate SIS and TIS are

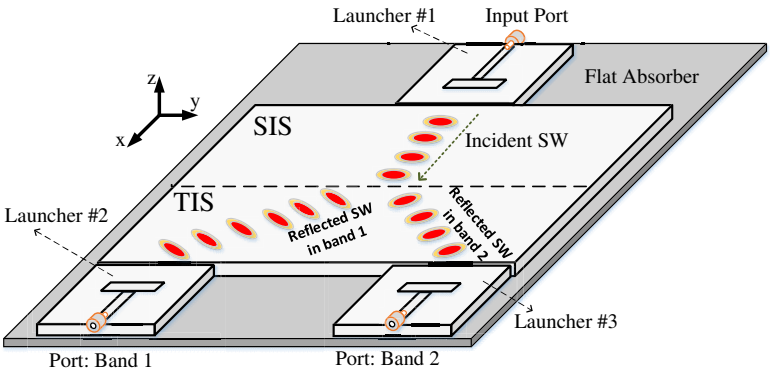

Figure 1. The proposed structure for SW diplexer.

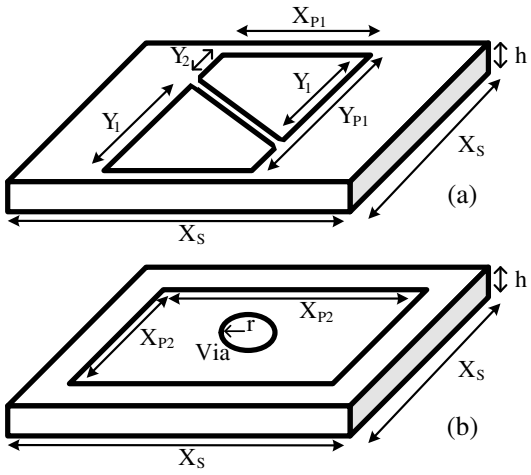

Figure 2. Geometry of the proposed cells, (a) anisotropic for the TIS, (b) isotropic for the SIS.

needed. A TIS is an impedance surface, and the impedance tensor is defined as Eq. (1).

$$\bar{\bar{Z}}_{surf} = \begin{bmatrix} Z_{xx} & Z_{xy} \\ Z_{yx} & Z_{yy} \end{bmatrix} \tag{1}$$

These two surfaces are obtained by the proper selection of two isotropic and non-isotropic cells that have a good bandwidth [14]. The geometry of the cells and their dimensions are shown in Fig. 2 and Table 1. The proposed structure is an array of these cells, which is fabricated by a RO4003 Rogers substrate with a relative permittivity of 3.55.

Table 1. Dimensions of the proposed cells (in millimeters).

h	X_S	X_{P1}	Y_{P1}	X_{P2}	r	Y_2	Y_1
0.8	4	2.1	3.75	2	0.5	1	2.55

These two cells are designed to have the highest bandwidth with reactive impedance in the single mode. Moreover, to minimize the losses due to the impedance mismatch between the surfaces, the dimensions and geometry of the SIS cell are selected using Eq. (2) [14, 15]

$$Z_{xx}Z_{yy} - Z_{xy}^2 = \eta^2 \tag{2}$$

where η is the surface impedance of the SIS. In Fig. 3, the dispersion diagrams of both cells are plotted for the TM and TE modes in various propagation directions. In this figure, it is clear that the minimum TE cut-off frequency is 21.5 GHz, which occurs at 90 degrees, and this frequency for the other SW propagation angles of TE modes is higher. On the other hand, the minimum excitation frequency of the TM mode, as shown in Fig. 3, is equal to 10.013 GHz. Therefore, the bandwidth of the structure in which the SW can propagate on the surface at all propagation angles is equal to 10.013–21.5 GHz. To ensure that the TIS is in single-mode operation, frequency margins should be considered at the beginning and end of this bandwidth.

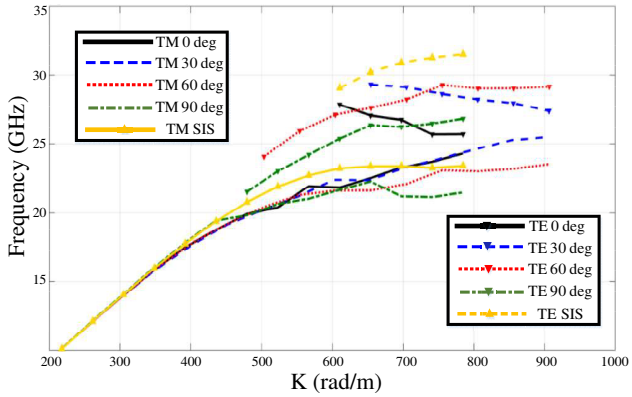

Figure 3. The dispersion diagrams of the TM and TE modes for the presented anisotropic and isotropic cells in different SW propagation angles.

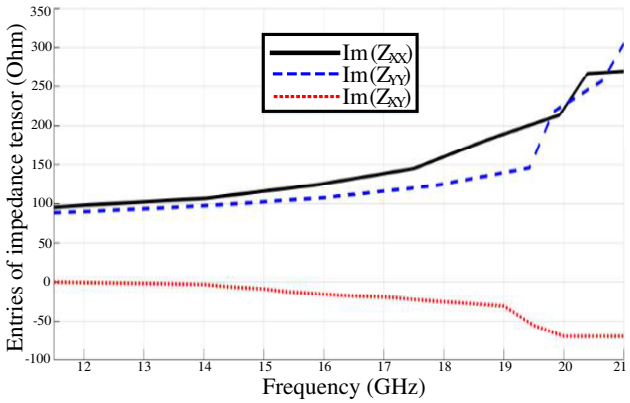

Figure 4. Imaginary part of entries of surface impedance tensor vs. frequency.

In Fig. 4, the entries of the surface impedance tensor of the TIS are shown. According to this figure, at the start of the frequency bandwidth, due to the equality of Z_{xx} and Z_{yy} and the small value of Z_{xy}, the surface exhibits isotropic behaviour. The non-isotropic manner of the TIS starts from 14 GHz. Therefore, the TIS shows non-isotropic behaviour in its single-mode bandwidth only within the range of 14–21 GHz.

Now according to Fig. 1, if the SW is excited on the SIS and crosses the TIS boundary vertically, it will enter the TIS with angle θ_k due to the refraction phenomenon. This refractive angle is a function of the SW frequency and is calculated as Eq. (3) [14]

$$\theta_k = \tan^{-1}\left\{\frac{2K_z'' Y_{xy}}{2K_z'' Y_{xx} + \dfrac{K_0}{Y_0}\left(Y_0^2 + det\bar{\bar{Y}}_{surf}\right)}\right\} \tag{3}$$

In Eq. (3), θ_k is the refraction angle of the SW; K_z'' is the component of the SW phase vector on the TIS along the z-axis; K_0 is the phase constant in the free space, and Y_0 is the free space admittance. Moreover, $\bar{\bar{Y}}_{surf}$ is the surface admittance tensor and is defined as Eq. (4).

$$\bar{\bar{Y}}_{surf} = \bar{\bar{Z}}_{surf}^{-1} = \begin{bmatrix} Y_{xx} & Y_{xy} \\ Y_{yx} & Y_{yy} \end{bmatrix} \tag{4}$$

3. CALCULATION OF INSERTION LOSS

There are three types of losses on the proposed structure: the losses due to the TM to TE mode conversion, the mismatch between the surface impedances of SIS and TIS, and the finite coupling efficiency of SW launchers [15]. Each TIS has two orthogonal propagation axes. When the SW propagates on the TIS axis, the modes are pure TM or TE. If the wave enters the TIS with angle θ_k relative to the main axis of the TM mode, a percentage of the TM mode will be converted to

TE, and due to the single-mode design of the surface, the wave radiates from the surface. Therefore, more mode conversion will result in more L_{MT} losses. This parameter is one of the limiting factors of increasing the refractive angle on the TISs. On the other hand, if the SW crosses the boundary of TIS and SIS, due to the mismatch between the surface impedances, a part of the wave will be reflected and causes another loss which is called the mismatch loss L_{MM} [15]. In Fig. 5, the L_{MM} and L_{MT} curves of the proposed structure are plotted using Eqs. (5) and (6).

$$L_{MM} = 1 - |\Gamma|^2 \tag{5}$$

In Eq. (5), Γ is the SW reflection coefficient at the boundary of TIS and SIS.

$$\begin{aligned} L_{MT} \;=\; & \left(\left[1 - \hat{x}_{xy}^2 + \hat{x}_{xx}\hat{x}_{yy} + 2\hat{x}_{xy}\frac{1-4x^2}{1+x^2} + (\hat{x}_{yy} - \hat{x}_{xx})\frac{2x}{1+x^2} \right.\right. \\ & -\frac{1}{\sqrt{2}}\left\{ 2 + \hat{x}_{xx}^2 + \hat{x}_{yy}^2 + 2\hat{x}_{xy}^2 + 4\hat{x}_{xx}\hat{x}_{yy}\left(1 - \hat{x}_{xy}^2\right) \right. \\ & \left.\left. \left. -4\hat{x}_{xy}\left(\hat{x}_{xx} - \hat{x}_{yy}\right)\frac{1+x^4-6x^2}{\left(1+x^2\right)^2} + \left(4\hat{x}_{xy}^2 - \left(\hat{x}_{xx} - \hat{x}_{yy}\right)^2\right)\frac{4x-4x^3}{\left(1+x^2\right)^2} \right\}^{\frac{1}{2}} \right] \right. \\ & \left. / \left[2\left(1 - \hat{x}_{xy}^2 + \hat{x}_{xx}\hat{x}_{yy}\right) \right] \right)^2 \end{aligned} \tag{6}$$

where in (6)

$$x = \frac{2\left|k_z''\right|\hat{x}_{xy}}{k_0\left(1 - \hat{x}_{xx}\hat{x}_{yy} + \hat{x}_{xy}^2\right) - 2\left|k_z''\right|\hat{x}_{yy}} \tag{7}$$

and $\hat{x}_{xx}$, $\hat{x}_{yy}$, and $\hat{x}_{xy}$ are the normalized entries of the surface reactance tensor; k_z'' is the normal component of the phase vector on the TIS, and k_0 is the wavenumber at the free space.

Figure 5 shows that due to the proper selection of the SIS cell and its surface impedance, the calculated mismatch loss is negligible. Another insertion loss in the structure is the result of the limitation of SW coupling on the surface and receiving from it. Coaxial probes are commonly used for SW measurements in the laboratory, but they cannot be employed for a microwave device such as a diplexer due to low coupling efficiency. Therefore, SW launchers are used for the proposed diplexer. To increase the SW coupling efficiency on the SIS, a substrate with high relative permittivity is needed [23, 24]. Therefore, for the launchers, a CER-10 Taconic substrate with a relative permittivity equal to 10 and a thickness of 0.8 mm is utilized. Fig. 6 shows the geometry of the proposed launcher.

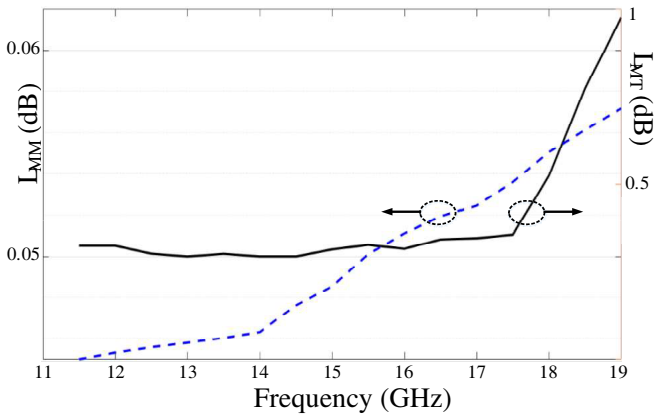

Figure 5. L_{MM} and L_{MT} of the proposed structure vs. frequency.

To increase the out-of-band rejection of the proposed diplexer, three types of this launcher are designed and tuned, which have different frequency characteristics. In Table 2, the dimensions of the proposed launchers are shown.

Table 2. The dimensions of the SW launchers (dimensions are in mm).

L_{L1}	L_{L2}	L_{L3}	W_{L1}	W_{L2}	L_{L4}	W_{LF}	W_{L4}	W_{L5}
15	1	6	30	0.9	0.9	0.5	4.5	0.5
Number of Launchers						W_{L6}	W_{L3}	L_{L5}
#1						7	4.5	3.1
#2						5.6	4.5	3.5
#3						6.2	3	3.1

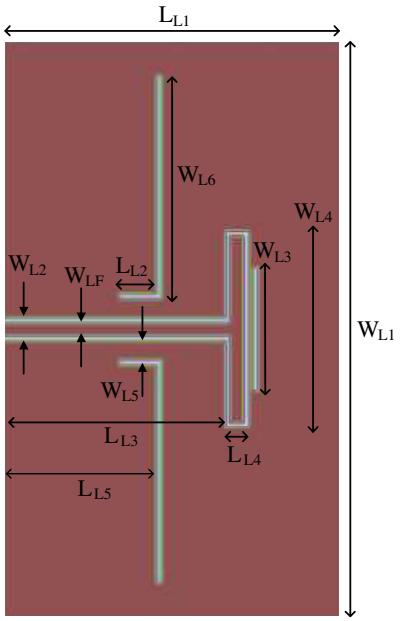

Figure 6. The geometry of proposed SW launchers.

The first launcher is designed for the input port of the structure, and in both frequency bands 11.6 and 19.3 GHz, it has suitable SW coupling efficiency and return loss. The second and third launchers are designed only for bands 1 and 2, respectively. In Figs. 7 and 8, the simulated input reflection coefficient and coupling efficiency of each launcher are drawn.

According to these figures, the first launcher has 88% SW coupling efficiency at 11.6 GHz and 87% at 19.3 GHz. Therefore, this launcher has a good performance in both frequency bands. Moreover, the coupling efficiency of the second and third launchers is more than 87%, respectively, in the first and second bands because these launchers are designed to have low coupling efficiency in the other band in order to improve diplexer rejection as much as possible.

4. IMPLEMENTATION AND MEASUREMENTS

The main purpose of this paper is to propose an SW-based diplexer. Therefore, according to Fig. 1, a structure is designed and fabricated as a microwave device with three ports. Fig. 9 shows an image of the designed launchers.

By putting the results of Fig. 4 in Eq. (3), the frequency variations of the refraction angle are obtained, as shown in Fig. 10. Furthermore, the structure is evaluated according to the test setup presented in [14], and the results are in good agreement with the calculated results. According to this figure, the refraction angle varies from about 0 degrees at 11.6 GHz to 14.5 degrees at 19.3 GHz.

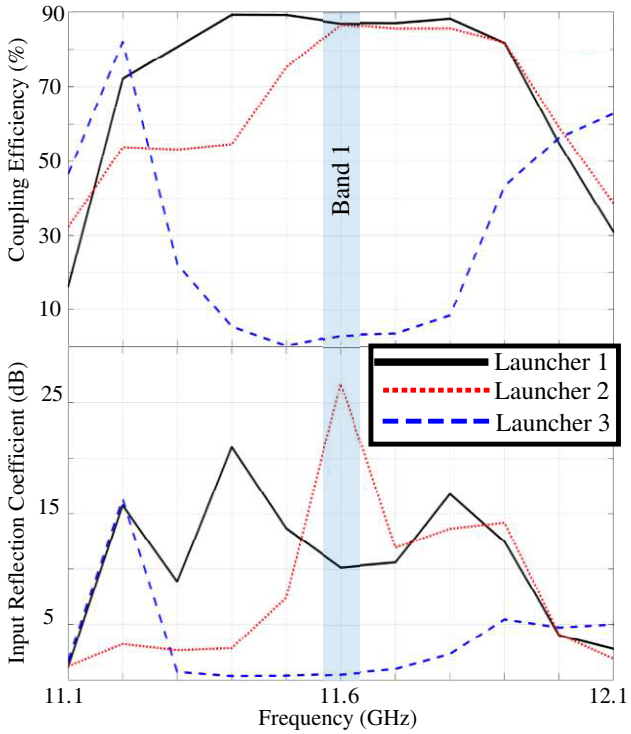

Figure 7. The simulated coupling efficiency and input reflection coefficient of the proposed SW launchers vs. frequency for the first band.

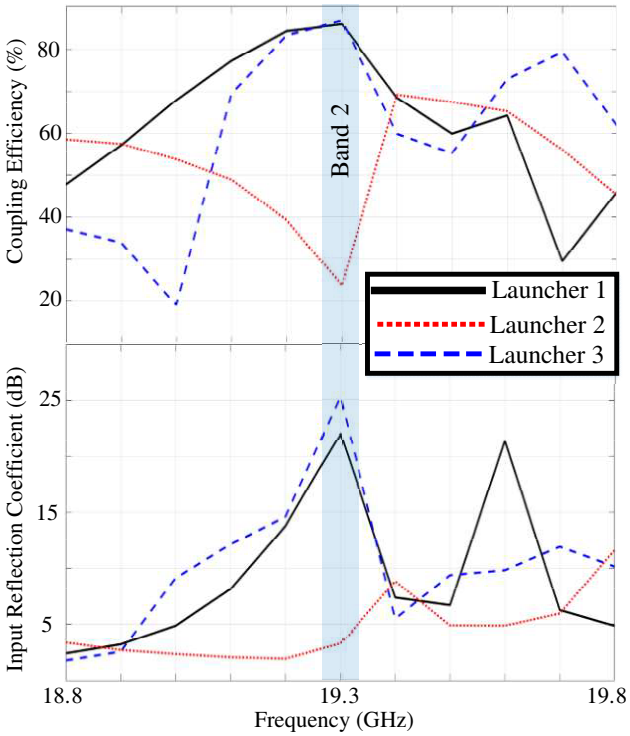

Figure 8. The simulated coupling efficiency and input reflection coefficient of the proposed SW launchers vs. frequency for the second band.

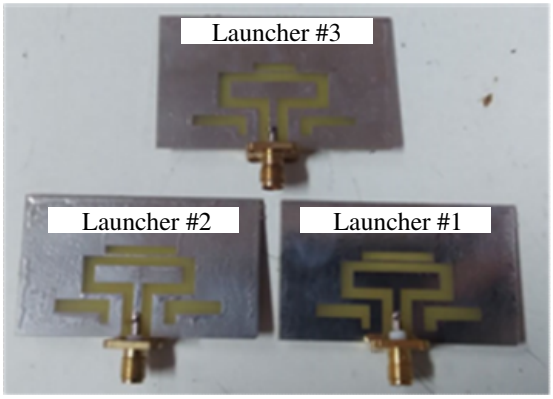

Figure 9. The photograph of the launchers.

Figure 11 shows the setup test that is used to measure the scattering parameters of the structure. In this test, R&S ZVA-24 vector network analyzer and a 50-ohm coaxial termination have been used as shown. Moreover, according to Fig. 11, in order to prevent unwanted SW scattering on the surface, a flat absorber, i.e., ECCOSORB BSR from Laird with 0.25 mm thickness, has been used.

As depicted in Fig. 1, the surface impedance sheet is implemented on a $150 \times 260\,\text{mm}^2$ Rogers RO4003 substrate. Fig. 12 shows the image of the measurement setup. Figs. 13 and 14 indicate the results of the measured input reflection coefficients of all ports in both bands. According to these figures, port 1, which is the input port of the diplexer, has a suitable impedance matching in the two frequency bands. Furthermore, ports 2 and 3, which are the outputs of the diplexer, are in the impedance matching conditions only at bands 1 and 2, respectively.

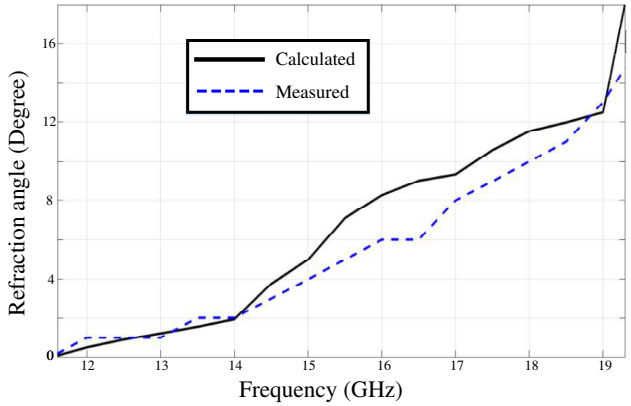

Figure 10. The Calculated and measured refraction angle of SW on the TIS.

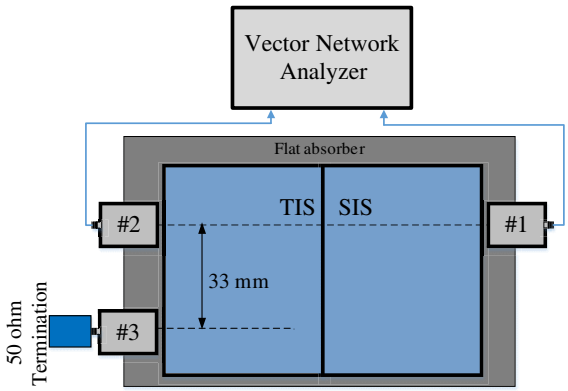

Figure 11. The presented setup for the measurements.

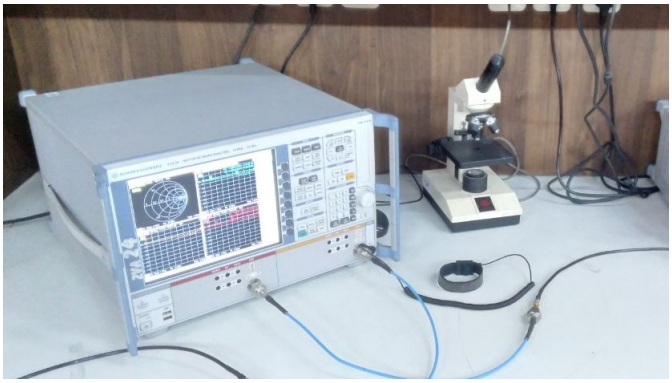

Figure 12. The photograph of the measurement setup.

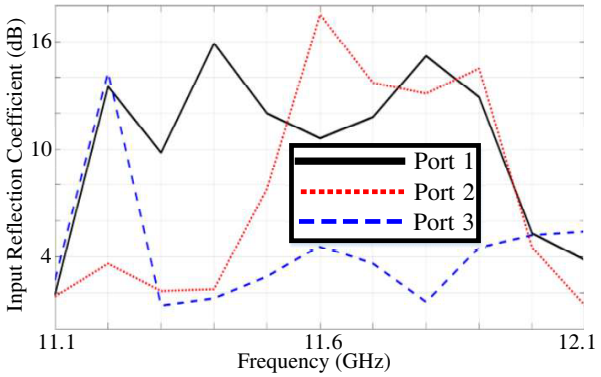

Figure 13. The measured input reflection coefficient in band 1.

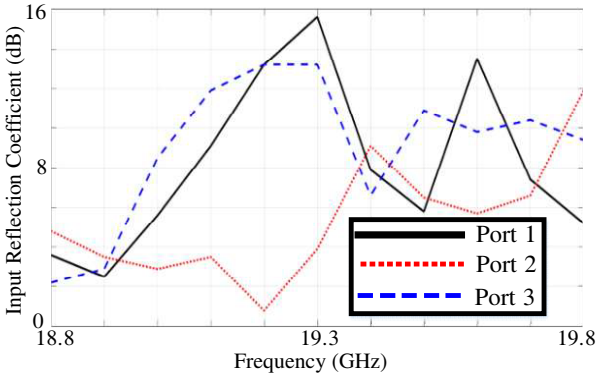

Figure 14. The measured input reflection coefficient in band 2.

In Fig. 15, the measured absolute values of S_{21} and S_{31} in band 1 are shown. According to this figure, the proposed diplexer has an insertion loss of 3.6 dB and an isolation of 37 dB at 11.6 GHz. Given the 88% coupling efficiency of the launchers and the losses modelled in Fig. 5, the measured insertion loss is predictable and in good agreement with the calculated results. The 37 dB isolation measured in this band is due to the refraction angle modelled in Fig. 10 and the 10% coupling efficiency of launcher 3 which is predicted in Fig. 7(a).

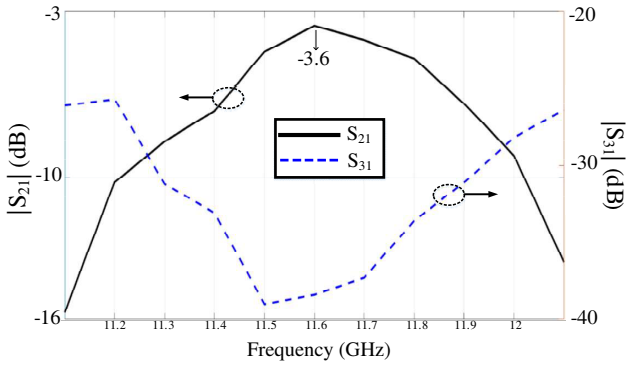

Figure 15. The measured absolute values of S_{21} and S_{31} in band 1.

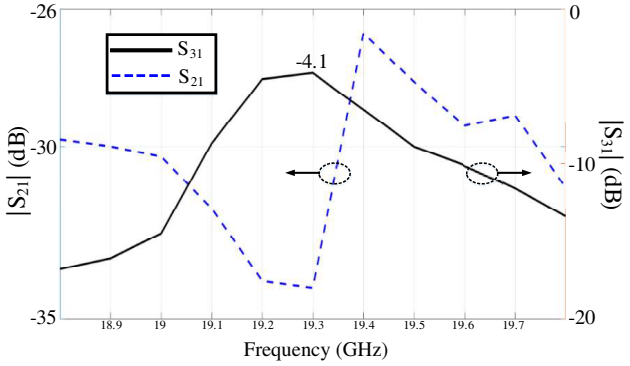

Figure 16. The measured absolute values of S_{21} and S_{31} in band 2.

In Fig. 16, the measured absolute values of S_{21} and S_{31} in band 2 are shown. According to this figure, the proposed diplexer has an insertion loss of 4.1 dB and an isolation of 33.5 dB at 19.3 GHz. Given the 87% coupling efficiency of the launchers and the mismatch and mode transform losses, which are modelled in Fig. 5, the measured insertion loss is predictable and in good agreement with the calculated results. The 33.5 dB isolation measured in this band is due to the modelled refraction angle in Fig. 10 and the 24% coupling efficiency of launcher 2 which is predicted in Fig. 8(a).

5. CONCLUSION

In this paper, a novel diplexer is presented based on the frequency variations of the refraction angle when SW enters a TIS from a SIS. This new structure is fabricated by placing a SIS alongside a TIS. Moreover, three different launchers have been used to excite the SW on the surface and receive from it. The results obtained from mathematical modelling and structure measurement are in good agreement. On the other hand, the validation of the possibility of creating an SW diplexer is one of the important findings of this paper.

REFERENCES

1. Matthaei, G. L., E. M. Jones, and L. Young, *Microwave Filters, Impedance-matching Networks, and Coupling Structures*, McGraw-Hill, New York, 1964.
2. Bushore, K. R. and W. L. Teeter, "A variable-ratio microwave power divider and multiplexer," *IRE Transactions on Microwave Theory and Techniques*, Vol. 5, No. 4, 227–229, Oct. 1957, doi: 10.1109/TMTT.1957.1125154.
3. Cristal, E. G. and G. L. Matthaei, "A technique for the design of multiplexers having contiguous channels," *IEEE Transactions on Microwave Theory and Techniques*, Vol. 12, No. 1, 88–93, Jan. 1964, doi: 10.1109/TMTT.1964.1125756.
4. Ricardi, L. J., "A diplexer using hybrid junctions," *IEEE Transactions on Microwave Theory and Techniques*, Vol. 14, No. 8, 364–371, Aug. 1966, doi: 10.1109/TMTT.1966.1126276.
5. Wang, R. and J. Xu, "Synthesis and design of microwave diplexers with a common resonator junction," *International Conference on Microwave and Millimeter Wave Technology (ICMMT)*, 1–4, Shenzhen, China, May 5–8, 2012, doi: 10.1109/ICMMT.2012.6230019.
6. Sorkherizi, M. S., et al., "Design of integrated diplexer-power divider," *IEEE MTT-S International Microwave Symposium (IMS)*, 1–3, San Francisco, CA, USA, May 22–27, 2016, doi: 10.1109/MWSYM.2016.7540124.
7. Song, K., et al., "Balanced diplexer based on substrate integrated waveguide dual-mode resonator," *IEEE Transactions on Microwave Theory and Techniques*, Vol. 68, No. 12, 5279–5287, Dec. 2020, doi: 10.1109/TMTT.2020.3015968.

8. Xu, J. X., et al., "Switchable diplexer based on coupling control," *IEEE Transactions on Circuits and Systems II: Express Briefs*, Vol. 68, No. 1, 166–170, Jan. 2021, doi: 10.1109/TCSII.2020.3003913.
9. Sieganschin, A., T. Jaschke, and A. F. Jacob, "A compact diplexer for circularly polarized 20/30 GHz SIW-antennas," *IEEE/MTT-S International Microwave Symposium (IMS)*, 599–602, Los Angeles, CA, USA, Aug. 4–6, 2020, doi: 10.1109/IMS30576.2020.9223900.
10. Yang, L., et al., "Input-reflectionless low-pass filter on multilayered diplexer-based topology," *IEEE Microwave and Wireless Components Letters*, Vol. 30, No. 10, 945–948, Oct. 2020, doi: 10.1109/LMWC.2020.3017252.
11. Xue, Y. M., et al., "Wideband diplexer with narrow channel spacing using hybrid bandpass-bandstop structures," *IEEE Access*, Vol. 8, 137783–137788, Jul. 27, 2020, doi: 10.1109/ACCESS.2020.3012348.
12. Macchiarella, G., et al., "A synthesis-based design procedure for waveguide duplexers using a stepped *E*-plane bifurcated junction," *IEEE/MTT-S International Microwave Symposium (IMS)*, 452–455, Los Angeles, CA, USA, Aug. 4–6, 2020, doi: 10.1109/IMS30576.2020.9223923.
13. García, J. O., et al., "Waveguide quadruplet diplexer for multi-beam satellite applications," *IEEE Access*, Vol. 8, 110116–110128, Jun. 16, 2020, DOI: 10.1109/ACCESS.2020.3002818.
14. Mighani, M. and G. Dadashzadeh, "Analytical study and experimental verification of the refraction angle as a function of frequency due to surface waves incident onto a tensor impedance sheet," *IEEE Transactions on Antennas and Propagation*, Vol. 67, No. 7, 4642–4649, Jul. 2019, doi: 10.1109/TAP.2019.2905779.
15. Mighani, M. and G. Dadashzadeh, "Analytical study and experimental verification of the surface wave loss on a tensor impedance surface," *Microwave and Optical Technology Letters*, Vol. 61, No. 12, 2879–2885, Dec. 2019, doi: 10.1002/mop.31983.
16. Mighani, M. and G. Dadashzadeh, "Analytical study of surface wave multiple refraction in boundary of a scalar impedance surface with a tensor impedance surface," *International Journal of RF and Microwave Computer-Aided Engineering*, Vol. 30, No. 4, 1–12, Jan. 2020, doi: 10.1002/mmce.22139.
17. Sievenpiper, D., et al., "High-impedance electromagnetic surfaces with a forbidden frequency band," *IEEE Transactions on Microwave Theory and Techniques*, Vol. 47, No. 11, 2059–2074, Nov. 1999, doi: 10.1109/22.798001.
18. Podilchak, S. K., et al., "Surface-wave launchers for beam steering and application to planar leaky-wave antennas," *IEEE Transactions on Antennas and Propagation,* Vol. 57, No. 2, 355–363, Feb. 2009, doi: 10.1109/TAP.2008.2011248.
19. Podilchak, S. K., et al., "Planar surface-wave sources and metallic grating lenses for controlled guided-wave propagation," *IEEE Antennas and Wireless Propagation Letters*, Vol. 8, 371–374, Jan. 2009, doi: 10.1109/LAWP.2009.2013488.
20. Mesa, F., C. di Nallo, and D. R. Jackson, "The theory of surface-wave and space-wave leaky-mode excitation on microstrip lines," *IEEE Transactions on Microwave Theory and Techniques*, Vol. 47, No. 2, 207–215, Feb. 1999, doi: 10.1109/22.744296.
21. Podilchak, S. K., et al., "Planar leaky-wave antenna designs offering conical-sector beam scanning and broadside radiation using surface-wave launchers," *IEEE Antennas and Wireless Propagation Letters*, Vol. 7, 155–158, Feb. 2008, doi: 10.1109/LAWP.2008.919326.
22. Bosiljevac, M., et al., "Non-uniform metasurface Luneburg lens antenna design," *IEEE Transactions on Antennas and Propagation*, Vol. 60, No. 9, 4065–4073, Sep. 2012, doi: 10.1109/TAP.2012.2207047.
23. Mahmoud, S. F., et al., "Theoretical considerations in the optimization of surface waves on a planar structure," *IEEE Transactions on Antennas and Propagation,* Vol. 52, No. 8, 2057–2063, Aug. 2004, doi: 10.1109/TAP.2004.832498.
24. Hammad, H. F., et al., "Uni-planar CPW-fed slot launchers for efficient TM_0 surface-wave excitation," *IEEE Transactions on Microwave Theory and Techniques*, Vol. 51, No. 4, 1234–1240, Apr. 2003, doi: 10.1109/TMTT.2003.809668.